Site-specific vibrational spectral signatures of water molecules in the magic $H_3O^+(H_2O)_{20}$ and $Cs^+(H_2O)_{20}$ clusters

Joseph A. Fournier[a], Conrad T. Wolke[a], Christopher J. Johnson[a,1], Mark A. Johnson[a,2], Nadja Heine[b], Sandy Gewinner[b], Wieland Schöllkopf[b], Tim Esser[c], Matias R. Fagiani[b,c], Harald Knorke[b,c], and Knut R. Asmis[c,2]

[a]Sterling Chemistry Laboratory, Yale University, New Haven, CT 06520; [b]Fritz-Haber-Institut der Max-Planck-Gesellschaft, D-14195 Berlin, Germany; and [c]Wilhelm-Ostwald-Institut für Physikalische und Theoretische Chemie, Universität Leipzig, D-04103 Leipzig, Germany

Contributed by Mark A. Johnson, October 30, 2014 (sent for review August 25, 2014; reviewed by David H. Russell and Sotiris S. Xantheas)

Theoretical models of proton hydration with tens of water molecules indicate that the excess proton is embedded on the surface of clathrate-like cage structures with one or two water molecules in the interior. The evidence for these structures has been indirect, however, because the experimental spectra in the critical H-bonding region of the OH stretching vibrations have been too diffuse to provide band patterns that distinguish between candidate structures predicted theoretically. Here we exploit the slow cooling afforded by cryogenic ion trapping, along with isotopic substitution, to quench water clusters attached to the H_3O^+ and Cs^+ ions into structures that yield well-resolved vibrational bands over the entire 215- to 3,800-cm^{-1} range. The magic $H_3O^+(H_2O)_{20}$ cluster yields particularly clear spectral signatures that can, with the aid of ab initio predictions, be traced to specific classes of network sites in the predicted pentagonal dodecahedron H-bonded cage with the hydronium ion residing on the surface.

water clusters | cryogenic vibrational spectroscopy | hydrogen bonding

Over the last decade, the cooperative mechanics underlying the microhydration of simple ions has undergone a renaissance due to rapid advances in experimental and theoretical methods. On the experimental side, it is routine to capture and study size-selected species cooled to cryogenic temperatures (1–5), and theoretical techniques are now capable of handling tens of atoms with all-electron, "supermolecule" approaches, where complex hydration networks are treated in the ansatz of polyatomic molecular physics (6). A dramatic example of the new insights afforded by this combined approach is the recent elucidation of the spectral signature associated with the hydronium ion when it is accommodated on the surface of a pentagonal dodecahedral cage formed by the "magic" $H_3O^+(H_2O)_{20}$ cluster (7). The theoretical structure proposed earlier (8) (denoted I) is illustrated in Fig. 1, and the recently reported D_2 predissociation spectra of the cryogenically cooled, D_2 tagged $H_3O^+(H_2O)_{20}$ cluster is compared with that observed for the $H_3O^+(H_2O)_3$ Eigen cation (9, 10) in Fig. 1 *A* and *B*, respectively. The key bands derived from the OH stretching motions of the surface-embedded hydronium (denoted $\nu^a_{H_3O^+}$) were assigned (7) to the broad features in the experimental spectrum about 500 cm^{-1} below the corresponding bands in the free Eigen cation. The intramolecular HOH bending and OH stretching modes of the surface water molecules are not strongly shifted by introduction of the ion, however, where the latter appear as a broad envelope spanning the 3,000- to 3,700-cm^{-1} range typical of liquid water. An interesting aspect of the D_2 tagged spectrum obtained with cryogenic cooling (as opposed to that reported on the same ion generated under the more rapid quenching conditions at play in a supersonic jet ion source) (8, 11) is that distinct features begin to emerge above the continuous background absorption in the OH stretching region above 3,400 cm^{-1}.

This observation of sharp OH stretching structure in a moderately large water cluster is significant in the context of the ongoing, often controversial discussion regarding the origin of the diffuse OH stretching spectrum displayed by neat liquid water (12–14), as well as by dilute acids (15, 16). Indeed, over the last decade, intensive experimental (17, 18) and theoretical (19–21) efforts have addressed the underlying mechanics of this broadening, resulting in significant differences of opinion regarding the role of excitonic band structure, excited state dynamics, and Fermi resonances (22–25). Cluster behavior is highly relevant in this discussion as they allow one to isolate microscopic assemblies with well-defined H-bonding configurations and thus directly address the spectral signatures associated with the various network morphologies. In this paper, we contrast the behavior of the $n = 20$ hydrates of the H_3O^+ and Cs^+ ions, both of which are preferentially generated in the $M^+(H_2O)_n$ cluster ion distributions (i.e., are magic numbers) and are thought to be based on a pentagonal dodecahedron motif (12 interconnected H-bonded pentagons). An important difference between these ions is that H_3O^+ is predicted to reside on the surface of the cage (6, 8, 26), whereas Cs^+ is sequestered in its interior (27, 28). We follow the evolution of the bands in the perdeuterated isotopologues, $Cs^+(D_2O)_{20}$ and $D_3O^+(D_2O)_{20}$, and find strong support for the earlier assignment of the spectral signature of the embedded H_3O^+ ion. Of most importance here, however, is the observation that the perdeuterated isotopologues yield

Significance

Understanding the mechanics underlying the diffuse OH stretching spectrum of water is a grand challenge for contemporary physical chemistry. Water clusters play an increasingly important role in this endeavor, as they allow one to freeze and isolate the spectral behavior of relatively large assemblies with well-defined network morphologies. We exploit recently developed, hybrid instruments that integrate laser spectroscopy with cryogenic ion trap MS to capture the H_3O^+ and Cs^+ ions in cage structures formed by 20 water molecules. Their infrared spectra reveal a pattern of distinct transitions that is unprecedented for water networks in this size range. Theoretical analysis of these patterns then reveals the intramolecular distortions associated with water molecules at various sites in the 3D cages.

Author contributions: M.A.J. and K.R.A. designed research; J.A.F., C.T.W., C.J.J., N.H., S.G., W.S., T.E., M.R.F., and H.K. performed research; J.A.F., C.T.W., C.J.J., M.A.J., N.H., S.G., W.S., T.E., M.R.F., H.K., and K.R.A. analyzed data; and J.A.F., C.T.W., C.J.J., M.A.J., N.H., S.G., W.S., T.E., M.R.F., H.K., and K.R.A. wrote the paper.

Reviewers: D.H.R., Texas A&M University; and S.S.X., Pacific Northwest National Laboratory.

The authors declare no conflict of interest.

[1]Present address: Department of Chemistry, Stony Brook University, Stony Brook, NY 11794.

[2]To whom correspondence may be addressed. Email: mark.johnson@yale.edu or knut.asmis@uni-leipzig.de.

This article contains supporting information online at www.pnas.org/lookup/suppl/doi:10.1073/pnas.1420734111/-/DCSupplemental.

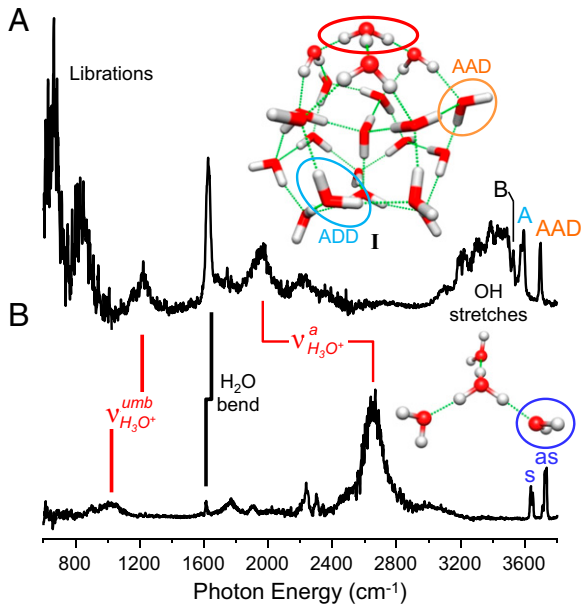

Fig. 1. Vibrational predissociation spectra of (*A*) $H_3O^+(H_2O)_{20}$ and (*B*) the $H_3O^+(H_2O)_3$ Eigen cation. Bands attributed (7) to the antiymmetric H_3O^+ stretches, $\nu^{a}_{H_3O^+}$, and H_3O^+ umbrella bending mode, $\nu^{umb}_{H_3O^+}$ of the embedded hydronium ion are indicated by the red lines. The antiymmetric stretches of remote ADD type waters (circled in turquoise in *A*) were assigned (6, 7) to band A, whereas the free OH stretches from the AAD waters are circled in orange. The symmetric (s) and antiymmetric (as) OH stretches of the water molecules solvating the Eigen cation (circled in blue) are expected (7) to red shift into the broad continuum near position B in $H_3O^+(H_2O)_{20}$. The $H_3O^+(H_2O)_{20}$ structure, denoted I, was the lowest energy structure identified in a search using the B3LYP method (6, 8).

significantly better resolved fine structure in the lower energy OD stretching manifold than was evident in the $H_3O^+(H_2O)_{20}$ spectrum. Comparison of this pattern with harmonic predictions yields compelling assignments of the strongest transitions to four classes of water molecules, which, in turn, allows us to refine the $H_3O^+(H_2O)_{20}$ structure I suggested earlier. Special aspects of the $n = 20$ structures are further investigated in a study of the low frequency (<1,000 cm^{-1}) librational motions over the size range n = 17–27, where significantly sharper structure is observed in the $n = 20$ spectrum relative to that displayed by nearby cluster sizes. The origin of these bands is considered in the context of harmonic spectra predicted for the geometries identified through assignment of the OH/OD stretching band pattern. Features associated with frustrated rotations of the trapped H_3O^+ moiety, as well as of water molecules in four-coordinated network sites, are thus identified for the first time.

Results and Discussion

Comparison of the D_2 Tagged $H_3O^+(H_2O)_{20}$ and $Cs^+(H_2O)_{20}$ Spectra and Evolution of the Bands in the Perdeuterated Isotopologues. Fig. 2 presents the evolution of the D_2 tagged $H_3O^+(H_2O)_{20}$ and $Cs^+(H_2O)_{20}$ vibrational predissociation spectra on deuteration. The bands assigned to the antisymmetric hydronium OH stretch ($\nu^{a}_{H_3O^+}$) near 2,000 cm^{-1} (Fig. 2*A*, highlighted in red) are indeed observed to shift in the heavy isotopologue (Fig. 2*B*) to a location close to 1,600 cm^{-1}, as expected for the change in reduced mass. Moreover, the corresponding features are absent in the spectra of $Cs^+(D_2O)_{20}$ and $Cs^+(H_2O)_{20}$ displayed in Fig. 2 *C* and *D*, respectively. The OD stretching regions of both hydrates display very strong, well-resolved features just below the sharp free OD fundamentals (denoted AAD). In fact, the OD stretching spectrum of $Cs^+(D_2O)_{20}$ is striking in that sharp features appear throughout the entire H-bonded OD stretching range, whereas the lower energy part of the corresponding feature in the $D_3O^+(D_2O)_{20}$ spectrum is more congested.

The appearance of isolated and intense bands in the high energy OH/OD stretching regions of both the Cs^+ and hydronium cluster spectra is of great interest, as such simple patterns likely signal rather symmetrical structures, i.e., those in which many water molecules reside in similar network sites. One of these bands (A near 3,580 cm^{-1}) was evident in the spectra reported a decade ago (8) and was assigned to the water molecules circled in turquoise in Fig. 1*A*, which adopt ADD network sites (A denotes an H-bond acceptor and D a donor) in structure I. Note that these sites are near the bottom of the cage, rather removed from the H_3O^+ charge center at the top. More recently, Xantheas revisited the theoretical structures expected for the $H_3O^+(H_2O)_{20}$ system in a systematic survey of more than 50,000 locally stable structures (6). He identified the seven lowest energy arrangements, all of which occur with H_3O^+ ions on the surface of pentagonal dodecahedra with subtle variations of the detailed donor/acceptor configurations of the water molecules that make up each interconnected pentagonal H-bonded ring. The calculated patterns of harmonic OH stretching fundamentals were found to be sensitive to these local variations, and indeed based on this dependence, he concluded that the structure displayed in Fig. 3 (denoted II) was more consistent with the observed spectrum. Specifically, this arrangement does not display the strong (harmonic) low energy OH stretching transition near 2,800 cm^{-1} that is predicted for the originally proposed structure I, but is missing in the experimental spectrum (Figs. S1 and S2). Interestingly, the key change between these structures involves a concerted flipping motion of three AADD type sites (including the central H_2O) along with a remote ADD site of the H-bonded network while maintaining the same number (9) of free OH groups.

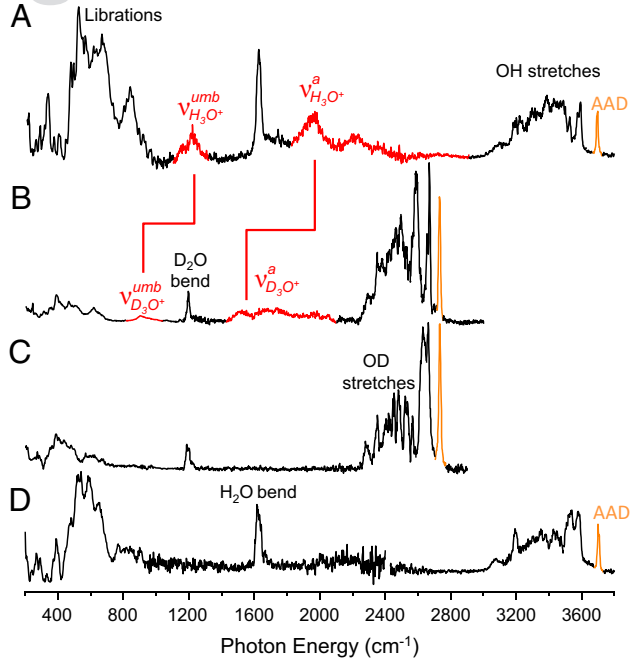

Fig. 2. Composite vibrational predissociation spectra of D_2 tagged ions taken with the Berlin FEL (<1,000 cm^{-1}) and the Yale table top system (1,000–3,800 cm^{-1}): (*A*) $H_3O^+(H_2O)_{20}$, (*B*) $D_3O^+(D_2O)_{20}$, (*C*) $Cs^+(D_2O)_{20}$, and (*D*) $Cs^+(H_2O)_{20}$. Bands attributed to the hydronium ion in *A* and *B* are highlighted in red and are clearly absent in the $Cs^+(D_2O)_{20}$ spectrum. Each spectra display a sharp free OH/OD stretching band highest in energy arising from AAD type water molecules (orange).

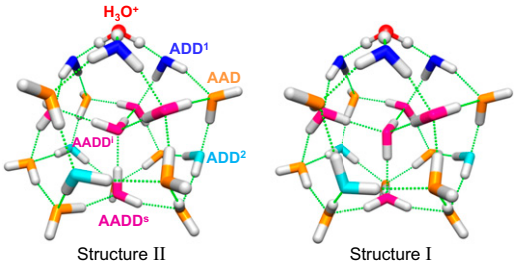

Fig. 3. Color-coded $H_3O^+(H_2O)_{20}$ structures for the MP2 minimum (structure II, *Left*) (6) and the B3LYP minimum (structure I, *Right*) (8). The H_3O^+ ion is colored red at the top of both structures. There are two classes of ADD waters: three (blue, ADD^1) solvate the hydronium ion and three (turquoise, ADD^2) are remote from the charge center. Colored in orange are the nine AAD type waters. Two classes of four-coordinate AADD molecules are colored pink: one in the interior (AADD^i) and four at the surface (AADD^s). The structural differences result from the reorientation of three of the five AADD molecules including the interior water.

Comparison with Harmonic Predictions: Structural Implications of the OH/OD Band Patterns. To clarify the assignments of the bands, we color code the various water molecules in structure II suggested by Xantheas in Fig. 3 and include a rotatable 3D structure in the *SI Materials and Methods* (structure I in Fig. S7 and structure II in Fig. S8). This structure exhibits approximate threefold symmetry evolving from the hydronium ion (red), with the three ADD water molecules (blue, denoted ADD^1) integrating the Eigen structure into the surface of the cage. Each of these bridging water molecules donates an H-bond to an AADD (pink) and an AAD (orange) molecule such that these orange AAD sites in turn link to the three lower ADD water molecules (turquoise, denoted ADD^2) farthest from the ion. Four of the four-coordinated AADD molecules reside on the surface (AADD^s) and one is sequestered in the interior (AADD^i).

The harmonic spectra for structure II are included in Fig. 4 *B* (all-H) and *D* (all-D). The AAD molecules (orange) yield a group of closely spaced transitions highest in energy that together account for the single observed free OH peak at the rather modest experimental resolution (3 cm^{-1}). The least red shifted H-bonding feature (A) now appears as an asymmetrical, closely spaced doublet with a shoulder on the low energy side, fine structure that is remarkably consistent with the harmonic prediction for structure II. OH displacements within the remote ADD^2 molecules (turquoise) are calculated to make the dominant contribution to the A feature with their antisymmetric stretching modes and account for the observed doublet structure in a scenario where one of these ADD^2 molecules is further topologically distinguished by its orientation relative to that of the interior water molecule (AADD^i). The corresponding symmetric stretching modes of the ADD^2 sites, on the other hand, are calculated to fall lower in energy where they merge with a dense series of more delocalized vibrations. In this scheme, the third strong feature (B) is largely due to the antisymmetric stretch of the primary hydronium solvation shell provided by the ADD^1 (blue) molecules. The antisymmetric stretch of the surface (AADD^s class, pink) molecules is also calculated to reside nearby and likely contributes to the broadening of the B feature.

The plausibility of these OH stretching assignments is strengthened by comparison with the observed and calculated $D_3O^+(D_2O)_{20}$ spectra in Fig. 4 *C* and *D*, respectively. The highest energy free OD singlet and A doublet are similar to those features in the all-H case. The analog of feature B, however, at 2,588 cm^{-1} emerges as a distinct band in the all-D spectrum [as opposed to blended with the blue edge of the continuous background absorption in the $H_3O^+(H_2O)_{20}$ spectrum]. This behavior is also anticipated by the harmonic prediction in the context of increased separation of the antisymmetric stretches arising from the ADD^1 (blue) molecules relative to the calculated symmetric stretches of the remote ADD^2 (turquoise) molecules.

Although it is clear that anharmonic effects will undoubtedly complicate this simple picture, it is nonetheless compelling that the three strong free OH/OD, A, and B bands (especially evident in the OD stretching spectrum) can be traced to particular classes of water molecules at play in the pentagonal dodecahedron: nine AAD, three ADD^1 (blue), and three ADD^2 (turquoise). Only the transitions involving the motions of the remaining five AADD molecules are masked by overlap with the strongly coupled, more distributed motions.

Having considered the assignment of key bands in the $D_3O^+(D_2O)_{20}$ spectrum to particular network sites in the pentagonal dodecahedron, it is useful to compare its spectrum to that of the $Cs^+(D_2O)_{20}$ cluster. Two reported minimum energy structures (29) of the metal ion cage are displayed in Fig. 5 along with the corresponding harmonic predictions (note that non-dodecahedral structures have also been shown to be nearly isoenergetic (27, 30) and high-level ab initio searches have yet to be performed on this system). Both arrangements have 10 AAD type molecules colored in orange. The remaining 10 ADD molecules are further differentiated into three classes according to the nature of the H-bond donor and acceptor molecules. The three ADD^1 sites (colored purple) are distinct because they accept

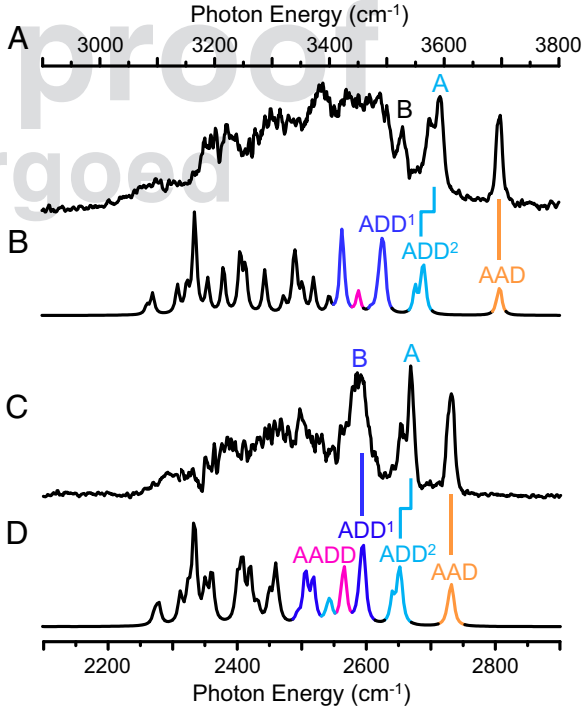

Fig. 4. Comparison of the experimental OH/OD stretching regions of (*A*) $H_3O^+(H_2O)_{20}$ and (*C*) $D_3O^+(D_2O)_{20}$ to the harmonic predictions for structure II in *B* and *D*, respectively. The top abscissa corresponds to the all-H spectra in *A* and *B*, whereas the bottom abscissa is associated with the all-D spectra in *C* and *D*. The spectra calculated for structure II are color-coded to identify sites whose displacements contribute most to the fundamental transitions. The free OH/OD stretches of AAD waters (orange) appear highest in energy, whereas feature A is traced to the antisymmetric stretches of the remote ADD water molecules (AAD^2, turquoise). The broad continuum near feature B in $H_3O^+(H_2O)_{20}$ resolves into a distinct band at 2,588 cm^{-1} on deuteration. The calculations indicate feature B may be due to the antisymmetric stretches of the water molecules (AAD^1, blue) in the first solvation shell around the hydronium ion. All calculated spectra [B3LYP/6–31+G(d)] were scaled by 0.973 to bring the free OH/OD stretches into agreement with those observed.

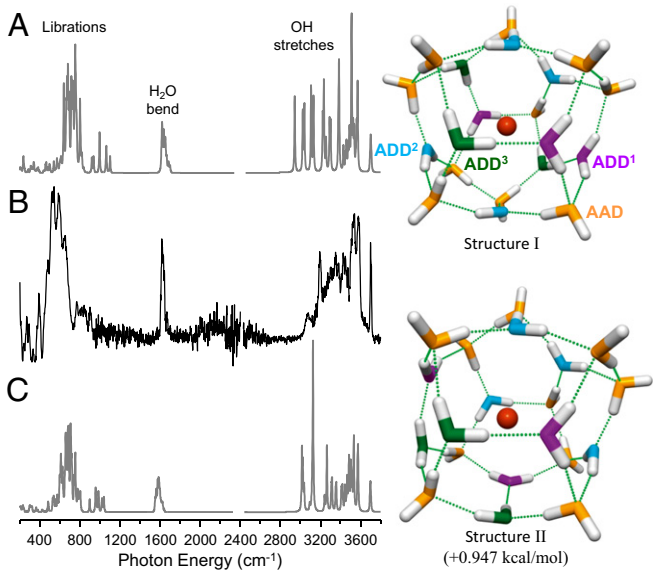

Fig. 5. Overview of the $Cs^+(H_2O)_{20}$ harmonic predictions for two minimum energy structures reported in ref. 29 in traces *A* and *C* compared with the experimental spectrum in *B*. Both calculated structures are pentagonal dodecahedra with the Cs^+ located in the center of the cage. Colored in orange are the ten AAD type water molecules. The ten remaining water molecules make up three distinct ADD type sites which depend on the local H-bonding environment. These are labeled ADD^1 (purple), ADD^2 (turquoise), and ADD^3 (green).

an H-bond from an ADD^3 molecule (green) while donating both H-bonds to AAD type waters (orange). The three ADD^3 sites (green) accept and donate an H-bond to AAD waters while donating the second H-bond to an ADD^1 water. The four ADD^2 (turquoise) waters are bound to three AAD molecules. As such, although one might have suspected that the pentagonal dodecahedron for the alkali ion might have been simpler than that formed around H_3O^+, calculations suggest that there are, in fact, more distinct sites in play.

The harmonic spectrum for the two calculated $Cs^+(D_2O)_{20}$ structures in Fig. 5 are presented in Fig. 6 *A* and *C*, respectively. The single feature highest in energy is accounted for by the nearly degenerate free OD stretches of the 10 AAD molecules (orange), whereas the ADD waters in $Cs^+(H_2O)_{20}$ are much less spectroscopically distinct compared with the two classes of ADD type molecules seen in $H_3O^+(H_2O)_{20}$ and lead to nearly overlapping transitions. Based on the calculated spectra, the sharp feature at 2,661 cm^{-1} can be traced to the antisymmetric OD stretches of the three ADD^1 water molecules colored in purple. The broader feature centered at 2,630 cm^{-1} then derives from the overlap of the antisymmetric OD stretches of the ADD^2 and ADD^3 waters.

In essence, the most important aspect of this exercise is to emphasize that the structure in the cryogenically cooled clusters is sufficiently well resolved to warrant such an attempt to identify the local sites responsible for the distinct bands. Unambiguous assignment will clearly require much more sophisticated theoretical treatment beyond the scope of this report, and it is indeed hoped that these results provide strong motivation for such efforts.

Survey of the Librational Bands from 200 to 1,000 cm^{-1}: Site-Specific H-Bonding Environments and Unique Behavior of $H_3O^+(H_2O)_{20}$. Our analysis of the $H_3O^+(H_2O)_{20}$ spectrum suggested that the fundamentals from the five AADD type (pink) molecules fall in a congested region of the OH/OD stretching manifold, and as such, are not expected to yield clear spectral signatures. Another aspect of the network environment of the AADD water molecules, however, is the strength of interaction with the surrounding cage that is associated with their fully saturated H-bonding. It is anticipated that the bands in the low energy region (<1,000 cm^{-1}) would effectively report on this local H-bonding environment (31). The low energy portion of the spectrum associated with water librational motion has not been explored for these intermediate cluster sizes, but it is accessible with high power infrared free electron lasers as recently demonstrated by Asmis and coworkers in a study of the $H^+(H_2O)_6$ ion (32). Here we survey the behavior of selected clusters in the n = 17–27 range over the region 215–1,000 cm^{-1}, with the results collected in Fig. 7. The low binding energy of H_2 (300 cm^{-1}) (11) onto protonated water clusters ensures that single photon (linear) spectra can be obtained overly nearly the complete spectral range investigated. All spectra in this size range display rather broad absorption envelopes with the exception of n = 20, which exhibits several distinct features throughout the range. The absorption peaks near 600 cm^{-1} and resolves into a multiplet at n = 20 before collapsing back to a single envelop at n = 27. The fine structure on the n = 20 spectrum strongly suggests that the ion ensemble is dominated by a single conformer class with rather high symmetry. This conclusion is consistent with the cage arrangement II depicted in Fig. 3, proposed based on the OH/OD stretching band patterns as described above.

To better gauge the types of motion involved in the low energy region of the spectrum, Fig. 8 *A* and *D* presents the harmonic predictions for both n = 20 cations along with their experimental spectra from 215 to 1,800 cm^{-1} (Fig. 8 *B* and *C*). Although it is clear that the calculated fundamentals lie higher in energy than the observed bands, it is nonetheless of qualitative interest to examine the normal modes yielding most oscillator strength in this low-frequency region. Representative displacement vectors for several strong fundamentals contributing to the calculated $H_3O^+(H_2O)_{20}$ spectrum are included in Fig. 8*A*. These are denoted 1–6 and colored according to the scheme outlined above according to the network sites most active in the calculated normal mode.

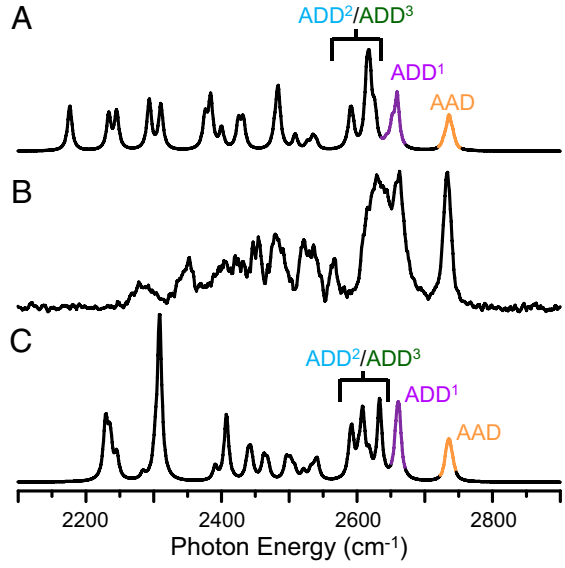

Fig. 6. Harmonic vibrational spectrum of (*A*) structure I and (*C*) structure II and that observed for $Cs^+(D_2O)_{20}$ in *B*. The highest energy feature is easily assigned to the free OD stretches of the AAD water molecules (orange). The ADD^1 water molecules (purple) are predicted to yield the narrower feature at 2,661 cm^{-1}, whereas the ADD^2 and ADD^3 sites (turquoise and green) overlap to yield the broader band at 2,630 cm^{-1}.

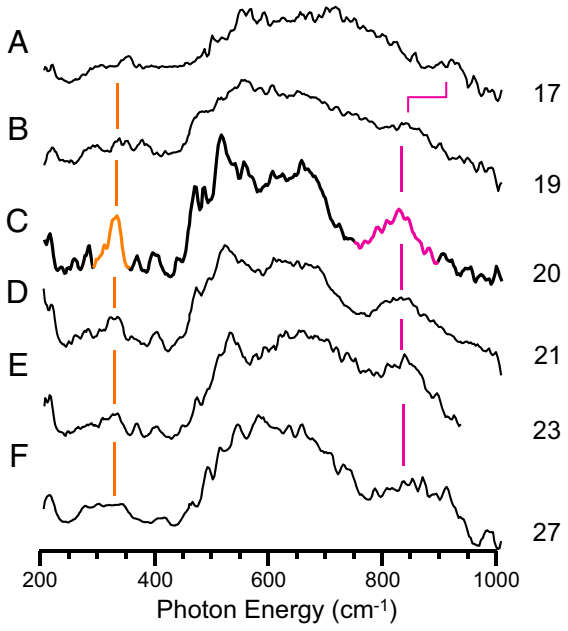

Q:18 **Fig. 7.** Vibrational spectra of the low energy librational modes collected using the FHI free electron laser for the indicated $H_3O^+(H_2O)_n$ clusters. Interestingly, the librational modes for $n = 20$ are more intense and better resolved compared with the other cluster sizes, perhaps due to the pentagonal dodecahedral symmetry. The positions of these modes should be indicators for the local H-bonding environment. The 341 (orange) and 842 cm^{-1} (pink) features observed in each cluster, for example, likely result from lower and higher H-bond coordination sites within the 3D cage structures, respectively.

Thus, feature 1 is associated mainly with the twisting motion of water molecules in AADD sites. Two modes arising from motions of the hydronium ion are colored red: one from frustrated rotation about the C_3 axis (feature 2) and one from rocking against the solvation shell (feature 3). Also in this energy range, and much weaker, are librational modes traced to motions of the bound hydrogens of AAD type waters (not labeled). With this in mind, we tentatively attribute the prominent feature (labeled † in Fig. 8*B*) near 850 cm^{-1} to H_3O^+ and four-coordinate AADD librational modes. Interestingly, the activity near 900 cm^{-1} in the $Cs^+(H_2O)_{20}$ spectrum (Fig. 8*C*) appears much weaker and less resolved than in $H_3O^+(H_2O)_{20}$, consistent with the absence of the H_3O^+ and AADD motifs in the metal system. The weaker transitions in this range for the Cs^+ cluster are mostly due to tortional motion of the AAD bound hydrogen as illustrated in Fig. 8*D*.

The strongest librational activity in the $H_3O^+(H_2O)_{20}$ spectrum (features 4 and 5 in Fig. 8*A*) is derived from the two classes of ADD molecules, with the waters directly solvating the hydronium (ADD^1) falling higher in energy than those (ADD^2) in the more remote site. The predicted envelope is in qualitative agreement with the observed multiplet spanning the range from 500 to 700 cm^{-1}. Interestingly, the corresponding ADD modes in $Cs^+(H_2O)_{20}$ (Fig. 8*D* and Fig. S3) occur in the same range and would similarly account for the multiplet structure that dominates that spectrum near 600 cm^{-1}. Finally, the lowest observed band at 341 cm^{-1} in $H_3O^+(H_2O)_{20}$ is in good agreement with predicted feature 6 (Fig. 8*A*), which is calculated to involve motions of the AAD free hydrogens, with the corresponding transition in $Cs^+(H_2O)_{20}$ appearing at 401 cm^{-1}. It is interesting to note that the librational modes of these free hydrogens are relatively sharp, isolated bands as was the case with the corresponding free OH stretches at 3,700 cm^{-1}. This localization of oscillator strength from a feature derived from so many oscillators [9 for $H_3O^+(H_2O)_{20}$ and 10 for $Cs^+(H_2O)_{20}$] is again easily rationalized by the relatively high symmetry of the pentagonal dodecahedron structures.

Conclusions

Cryogenic cooling of the size-selected $H_3O^+(H_2O)_n$ ($17 < n < 27$) cluster ions, in conjunction with D_2 tagging and isotopic substitution, yields unprecedented structure in their vibrational predissociation spectra, both in the higher-frequency region corresponding to OH stretching and the lower-frequency region arising from librational motions of water molecules trapped in various distinct network sites. The evolution of the $H_3O^+(H_2O)_{20}$ spectrum with H/D substitution, as well as on replacement of hydronium with Cs^+, provides strong support for the earlier assignment (7) of the spectral signature associated with the $H_9O_4^+$ Eigen cation embedded on the surface of a pentagonal dodecahedron cage structure. The low energy librational motions are reported for this class of systems for the first time, to our knowledge, and reveal site-specific features based on the local H-bond coordination and strength. The observation of highly articulated band patterns for these hydrates opens the way for rigorous characterization of the structures at play at the

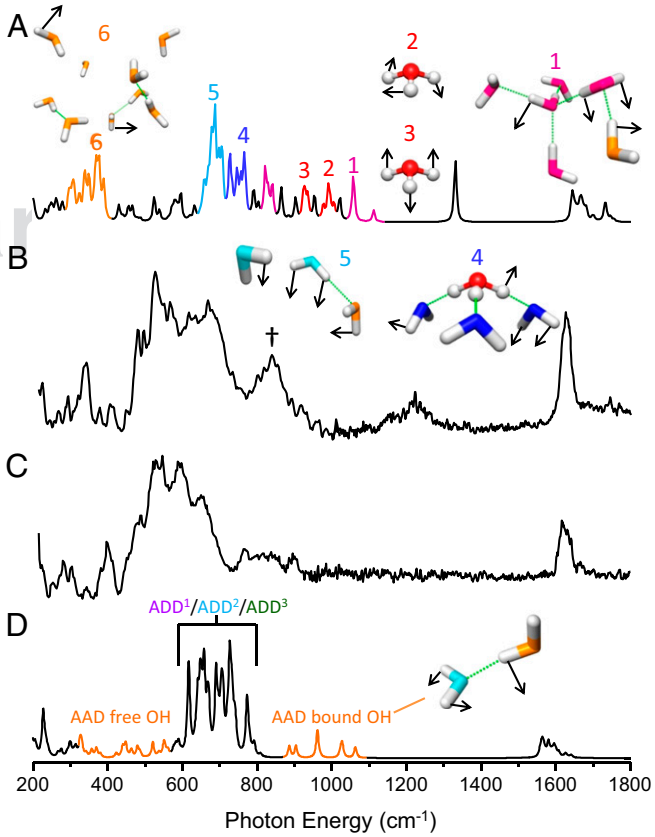

Fig. 8. Comparison of the 200- to 1,800-cm^{-1} region of (*B*) $H_3O^+(H_2O)_{20}$ and (*C*) $Cs^+(H_2O)_{20}$ to those computed for the lowest energy structures in *A* and *D*, respectively. Displacement vectors are shown for the dominant $H_3O^+(H_2O)_{20}$ fundamentals indicated in *A*. The highest energy librational bands in $H_3O^+(H_2O)_{20}$ involve motion of the AADD type waters (feature 1, pink) and frustrated rotations of the hydronium ion (features 2 and 3, red). For $Cs^+(H_2O)_{20}$, the weaker and broader bands near 1,000 cm^{-1} derive mostly from the bound AAD hydrogen. The dominant multiplets near 600 cm^{-1} in both spectra are mostly due to torsional motions of the multiple ADD sites (features 4 and 5). Lowest in energy are motions of the AAD free OH (orange).

elementary stages of ion hydration by explicitly including vibrational anharmonicity in the calculated band patterns.

Materials and Methods

Research carried out at Yale used the tandem time of flight photofragmentation mass spectrometer described previously (33) to acquire the vibrational spectra of the protonated water clusters cryogenically frozen close to their zero-point energy. Clusters were generated by electrospray ionization of 0.1% H_2SO_4 in a H_2O solution and D_2SO_4 in a D_2O solution for the all-H and all-D clusters, respectively. In the case of the $Cs^+(H_2O)_{20}/(D_2O)_{20}$ cluster, Cs_2CO_3 in H_2O/D_2O was used as the electrospray solution. The generated clusters were guided using RF-only quadrupole and octopole guides into a 3D quadrupole Paul trap (Jordan) mounted to the second stage of a 4 K closed cycle Helium cryostat. The ions were stored for ~90 ms, during which they are collisionally cooled by helium buffer gas. The buffer gas was doped with about 10% D_2, which condensed onto the cluster of interest at these cold temperatures and acted as the spectroscopic messenger (34). The cold clusters were ejected from the trap into the extraction region of a Wiley-McLaren TOF mass spectrometer.

Mass-selected ions were photoexcited with the output from a Nd:YAG pumped (7 ns, 10 Hz) OPO/OPA IR laser (LaserVision). The output of the OPA is tunable from 2,200 to 4,500 cm^{-1}, with a laser bandwidth of about 3 cm^{-1}. The lower energy 600- to 2,600-cm^{-1} region was produced by difference frequency mixing of the signal and idler output of the OPA in $AgGaSe_2$. The action spectra were collected by monitoring the single photon-induced evaporation of the D_2 molecule with respect to photon energy and normalized to the laser pulse energy to take account for fluctuations in the laser power during the scan.

Infrared photodissociation experiments in the lowest energy region (215–1,000 cm^{-1}) were carried out using the Berlin 6-K ion-trap triple mass spectrometer (35) in combination with the widely tunable and intense IR radiation from the new free electron laser (36) at FHI. Microhydrated ions were produced in a nanospray ion source. Protonated water clusters were generated as described above. $Cs^+(H_2O)_{20}/(D_2O)_{20}$ clusters were generated from a $CsCl/H_2O/D_2O$ solution. The continuous molecular beam was collimated using a He-filled RF-only octopole ion guide. After mass selection with a quadrupole mass filter, the ions were focused into a linear RF ring electrode ion-trap, which was kept at 13–14 K, to accumulate, thermalize, and D_2 messenger tag (37). Ion packets were extracted and focused in a 5-Hz cycle into the center of the extraction region of TOF mass spectrometer. Here, they were irradiated by the 7-μs-long IR macropulse of the FHI-FEL with typical bandwidths of 0.3–1% full width at half maximum (FWHM) of the central wavelength. Action spectra were recorded by averaging over 75–100 TOF mass spectra per wavelength step. Typically, a distribution of $(D_2)_m$-tagged cations, peaking at $m = 1$, were produced in the ion trap (Fig. S4). However, the differences between the action spectra of cations with a single ($m = 1$) and with more than one tag ($m > 1$) were negligible (Fig. S5), and therefore the ion yields of all tagged cations were summed up. The photodissociation cross section σ was then determined from the relative abundance of the fragment and parent ions (I_F/I_P) and the frequency-dependent laser fluence $F(\nu)$ using $\sigma(\nu) = -\ln\{[I_F(\nu)/I_P]\}/F(\nu)$.

All calculations were performed using the Gaussian 09 suite of programs (38) using the B3LYP/6–31+G(d) level of theory and basis. For the $Cs^+(H_2O)_{20}$ calculations, the LANL2DZ pseudopotential was used for Cs.

ACKNOWLEDGMENTS. M.A.J. thanks the US Department of Energy under Grant DE-FG02-06ER15800 for the work on the large protonated water clusters and the National Science Foundation under Grant CHE-1213634 for the work on Cs^+ hydration. Development of the Yale cryogenic ion spectrometer was supported by the US Air Force under Grant FA9550-13-1-0007. J.A.F. thanks the US Department of Defense for support through a National Defense Science and Engineering Graduate Fellowship. This work was supported in part by the facilities and staff of the Yale University Faculty of Arts and Sciences High Performance Computing Center and by the National Science Foundation under Grant CNS 08-21132 that partially funded acquisition of the facilities.

1. Wolk AB, Leavitt CM, Garand E, Johnson MA (2014) Cryogenic ion chemistry and spectroscopy. *Acc Chem Res* 47(1):202–210.
2. Rizzo TR, Stearns JA, Boyarkin OV (2009) Spectroscopic studies of cold, gas-phase biomolecular ions. *Int Rev Phys Chem* 28(3):481–515.
3. Wang XB, Xing XP, Wang LS (2008) Observation of H_2 aggregation onto a doubly charged anion in a temperature-controlled ion trap. *J Phys Chem A* 112(51):13271–13274.
4. Kim JB, Hock C, Yacovitch TI, Neumark DM (2013) Slow photoelectron velocity-map imaging spectroscopy of cold thiozonide (S3(-)). *J Phys Chem A* 117(34):8126–8131.
5. Goebbert DJ, Wende T, Bergmann R, Meijer G, Asmis KR (2009) Messenger-tagging electrosprayed ions: Vibrational spectroscopy of suberate dianions. *J Phys Chem A* 113(20):5874–5880.
6. Xantheas SS (2012) Low-lying energy isomers and global minima of aqueous nanoclusters: Structures and spectroscopic features of the pentagonal dodecahedron $(H_2O)_{(20)}$ and $(H_3O)^+(H_2O)_{(20)}$. *Can J Chem Eng* 90(4):843–851.
7. Fournier JA, et al. (2014) Vibrational spectral signature of the proton defect in the three-dimensional $H^+(H_2O)_{21}$ cluster. *Science* 344(6187):1009–1012.
8. Shin J-W, et al. (2004) Infrared signature of structures associated with the H+(H2O)n (n = 6 to 27) clusters. *Science* 304(5674):1137–1140.
9. Okumura M, Yeh LI, Myers JD, Lee YT (1986) Infrared spectra of the cluster ions $H_7O_3^+ \cdot H_2$ and $H_9O_4^+ \cdot H_2$. *J Chem Phys* 85:2328–2329.
10. Headrick JM, et al. (2005) Spectral signatures of hydrated proton vibrations in water clusters. *Science* 308(5729):1765–1769.
11. Mizuse K, Fujii A (2011) Structural origin of the antimagic number in protonated water clusters $H^+(H_2O)_{(n)}$: Spectroscopic observation of the "missing" water molecule in the outermost hydration shell. *J Phys Chem Lett* 2(17):2130–2134.
12. Auer BM, Skinner JL (2008) IR and Raman spectra of liquid water: Theory and interpretation. *J Chem Phys* 128(22):224511.
13. Auer B, Kumar R, Schmidt JR, Skinner JL (2007) Hydrogen bonding and Raman, IR, and 2D-IR spectroscopy of dilute HOD in liquid D_2O. *Proc Natl Acad Sci USA* 104(36): 14215–14220.
14. Paesani F, Xantheas SS, Voth GA (2009) Infrared spectroscopy and hydrogen-bond dynamics of liquid water from centroid molecular dynamics with an ab initio-based force field. *J Phys Chem B* 113(39):13118–13130.
15. Marx D, Tuckerman ME, Hutter J, Parrinello M (1999) The nature of the hydrated excess proton in water. *Nature* 397:601–604.
16. Knight C, Voth GA (2012) The curious case of the hydrated proton. *Acc Chem Res* 45(1):101–109.
17. Loparo JJ, Roberts ST, Tokmakoff A (2006) Multidimensional infrared spectroscopy of water. I. Vibrational dynamics in two-dimensional IR line shapes. *J Chem Phys* 125(19):194521.
18. Loparo JJ, Roberts ST, Tokmakoff A (2006) Multidimensional infrared spectroscopy of water. II. Hydrogen bond switching dynamics. *J Chem Phys* 125(19):194522.
19. Bakker HJ, Skinner JL (2010) Vibrational spectroscopy as a probe of structure and dynamics in liquid water. *Chem Rev* 110(3):1498–1517.
20. Skinner JL, Auer BM, Lin YS (2009) Vibrational line shapes, spectral diffusion, and hydrogen bonding in liquid water. *Adv Chem Phys* 142:59–103.
21. Rey R, Møller KB, Hynes JT (2004) Ultrafast vibrational population dynamics of water and related systems: A theoretical perspective. *Chem Rev* 104(4):1915–1928.
22. Ashihara S, Huse N, Espagne A, Nibbering ETJ, Elsaesser T (2007) Ultrafast structural dynamics of water induced by dissipation of vibrational energy. *J Phys Chem A* 111(5): 743–746.
23. Cowan ML, et al. (2005) Ultrafast memory loss and energy redistribution in the hydrogen bond network of liquid H2O. *Nature* 434(7030):199–202.
24. Laenen R, Simeonidis K, Laubereau A (2002) Time resolved spectroscopy of water in the infrared: New data and discussion. *Bull Chem Soc Jpn* 75(5):925–932.
25. De Marco L, Ramasesha K, Tokmakoff A (2013) Experimental evidence of Fermi resonances in isotopically dilute water from ultrafast broadband IR spectroscopy. *J Phys Chem B* 117(49):15319–15327.
26. Iyengar SS, et al. (2005) The properties of ion-water clusters. I. The protonated 21-water cluster. *J Chem Phys* 123(8):084309.
27. Cooper RJ, Chang TM, Williams ER (2013) Hydrated alkali metal ions: Spectroscopic evidence for clathrates. *J Phys Chem A* 117(30):6571–6579.
28. Schulz F, Hartke B (2003) Structural information on alkali cation microhydration clusters from infrared spectra. *Phys Chem Chem Phys* 5(22):5021–5030.
29. Schulz F, Hartke B (2002) Dodecahedral clathrate structures and magic numbers in alkali cation microhydration clusters. *ChemPhysChem* 3(1):98–106.
30. Smith DE, Dang LX (1994) Computer-simulations of cesium water clusters: Do ion water clusters form gas-phase clathrates. *J Chem Phys* 101(9):7873–7881.
31. Asmis KR, Neumark DM (2012) Vibrational spectroscopy of microhydrated conjugate base anions. *Acc Chem Res* 45(1):43–52.
32. Heine N, et al. (2013) Isomer-selective detection of hydrogen-bond vibrations in the protonated water hexamer. *J Am Chem Soc* 135(22):8266–8273.
33. Robertson WH, Kelley JA, Johnson MA (2000) A pulsed supersonic entrainment reactor for the rational preparation of cold ionic complexes. *Rev Sci Instrum* 71(12): 4431–4434.
34. Kamrath MZ, Relph RA, Guasco TL, Leavitt CM, Johnson MA (2011) Vibrational predissociation spectroscopy of the H_2-tagged mono- and dicarboxylate anions of dodecanedioic acid. *Int J Mass Spectrom* 300:91–98.
35. Heine N (2014) *Vibrational Spectroscopy of Gaseous Hydrogen-Bonded Clusters: On the Role of Isomer-Specificity and Anharmonicity* (Freie Universitat, Berlin).
36. Schöllkopf W, et al. (2013) The IR and THz free-electron laser at the Fritz-Haber-Institut. *Proceedings of the 35th International Free Electron Laser Conference*.
37. Brummer M, Kaposta C, Santambrogio G, Asmis KR (2003) Formation and photodepletion of cluster ion-messenger atom complexes in a cold ion trap: Infrared spectroscopy of VO^+, VO_2^+, and VO_3. *J Chem Phys* 119(24):12700–12703.
38. Frisch MJ, et al. (2009) *Gaussian 09, Revision D.01* (Gaussian, Wallingford, CT).

AUTHOR QUERIES

AUTHOR PLEASE ANSWER ALL QUERIES 1

Q: 1_Please contact PNAS_Specialist.djs@sheridan.com if you have questions about the editorial changes, this list of queries, or the figures in your article. Please include your manuscript number in the subject line of all email correspondence; your manuscript number is 201420734.

Q: 2_Please (i) review the author affiliation and footnote symbols carefully, (ii) check the order of the author names, and (iii) check the spelling of all author names, initials, and affiliations. Please check with your coauthors about how they want their names and affiliations to appear. To confirm that the author and affiliation lines are correct, add the comment "OK" next to the author line. This is your final opportunity to correct any errors prior to publication. Misspelled names or missing initials will affect an author's searchability. Once a manuscript publishes online, any corrections (if approved) will require publishing an erratum; there is a processing fee for approved erratum.

Q: 3_Please review and confirm your approval of the short title: Site-specific IR spectroscopy of water clusters. If you wish to make further changes, please adhere to the 50-character limit. (NOTE: The short title is used only for the mobile app and the RSS feed.)

Q: 4_Please review the information in the author contribution footnote carefully. Please make sure that the information is correct and that the correct author initials are listed. Note that the order of author initials matches the order of the author line per journal style. You may add contributions to the list in the footnote; however, funding should not be an author's only contribution to the work.

Q: 5_You have chosen not to pay an additional $1350 (or $1000 if your institution has a site license) for the PNAS open access option. Please confirm this is correct and note your approval in the margin.

Q: 6_Please verify that all supporting information (SI) citations are correct. Note, however, that the hyperlinks for SI citations will not work until the article is published online. In addition, SI that is not composed in the main SI PDF (appendices, datasets, movies, and "Other Supporting Information Files") have not been changed from your originally submitted file and so are not included in this set of proofs. The proofs for any composed portion of your SI are included in this proof as subsequent pages following the last page of the main text. If you did not receive the proofs for your SI, please contact **PNAS_Specialist.djs@sheridan.com**.

Q: 7_PNAS allows up to five keywords. You may add 2 keywords. Also, please check the order of your keywords and approve or reorder them as necessary.

Q: 8_If your article contains links to websites (other than the SI links for your article), please verify that the links are valid and will direct readers to the proper webpage.

Q: 9_Please provide department/section for all affiliations.

Q: 10_Per PNAS style, SI figures must be cited in order in the main text. Please cite Figs. S3-S6 and Fig. S9 in order in the text.

AUTHOR QUERIES

AUTHOR PLEASE ANSWER ALL QUERIES 2

Q: 11_PNAS mandates unambiguous pronoun antecedents. Please provide an appropriate noun after "These": "These are denoted...."

Q: 12_Please spell out OPA and IR.

Q: 13_Please spell out FHI.

Q: 14_Please spell out FEL.

Q: 15_For the following references, please provide the issue number: 9, 15, 20, and 34.

Q: 16_For ref. 36, please provide dates and location of conference, publisher, location of publisher (city and state/country), and page range.

Q: 17_PNAS mandates unambiguous pronoun antecedents. Please provide an appropriate noun after "These": "These are labeled...."

Q: 18_Per PNAS style, figure labels must be called out in the figure legend. Please provide descriptions for (A)-(F) in Figure 7.

Supporting Information

Fournier et al. 10.1073/pnas.1420734111

SI Materials and Methods

The Fritz Haber Institute Free Electron Laser. The IR pulses from the FHI-FEL consist of 5- to 8-μs-long pulse trains (macropulses) formed by thousands of few-picoseconds-long micropulses at a repetition rate of 1 GHz. The macropulse repetition rate was synchronized to the 5-Hz ion-trap extraction cycle. The Fourier-limited bandwidth of the FEL radiation was monitored with a Czerny-Turner type grating spectrometer. The relative bandwidth was found to be 0.35–0.6% in terms of the FWHM normalized to the central wavelength when lasing at 1,000 cm^{-1}, increasing to 1.0–1.5% FWHM at the longest wavelengths near 210 cm^{-1}. This corresponds to absolute FWHM bandwidths of 3.6–6 and 2–3 cm^{-1} Q:1 at central wavelengths of 1,000 and 210 cm^{-1}, respectively. In most of the measurements reported here, the macropulse energy of 10–35 mJ was reduced by several decibels by inserting IR attenuators into the FEL beam path upstream of the ion trap apparatus.

Fig. S1. Color-coded $D_3O^+(D_2O)_{20}$ structures and harmonic spectra for the (*A*) B3LYP minimum (structure I) and (*C*) MP2 minimum (structure II) compared with the observed in *B*. Red, hydronium; blue, hydronium-solvating ADD; turquoise, remote ADD; orange, AAD; pink, AADD. The structural differences result from rearrangement of the hydrogen bonding network, in particular, the reorientation of three of the five AADD molecules including the central water. The calculated spectrum for structure II is in better agreement with that observed and eliminates the most red shifted feature near 2,150 cm^{-1} predicted from structure I.

Fig. S1

Fig. S2. Overview of the $H_3O^+(H_2O)_{20}$ harmonic predictions for (*A*) structure II and (*C*) structure I compared with the (*B*) experimental spectrum. Structure I predicts one OH stretch (labeled *) at 2,950 cm^{-1} to be significantly red shifted, which is clearly absent in the experiment. Such a red shifted feature is not predicted for structure II. The calculated spectra [B3LYP/6–31+G(d)] were scaled by 0.973 to bring the free OH stretches into agreement with that observed.

Fig. S2

Fig. S3. Comparison of the computed librational modes of (*A*) structure I and (*C*) structure II to those observed in (*B*) $Cs^+(H_2O)_{20}$. The highest energy bands near 800 cm^{-1} (feature 1) derive mainly from the motion of the bound AAD hydrogens (orange). The strong suite of transitions near 600 cm^{-1} are predicted to result from the overlap of the three ADD types of water molecules (features 2 and 3). Lowest in energy are features due to the free AAD hydrogens (feature 4, orange).

Fig. S3

Fig. S4. TOF mass spectra of messenger-tagged (*A*) $H_3O^+(H_2O)_{20}$, (*B*) $D_3O^+(D_2O)_{20}$, (*C*) $Cs^+(H_2O)_{20}$, and (*D*) $Cs^+(D_2O)_{20}$ cations using the FHI ring electrode ion trap triple mass spectrometer. The mass spectra show the distribution of the weakly bound D_2 adducts onto the bare parent ions, peaking at a single tag but extending up to four tags.

Fig. S4

Fig. S5. Vibrational predissociation spectra of (*A*) $Cs^+(D_2O)_{20}$ tagged with two D_2 molecules, (*B*) $Cs^+(D_2O)_{20}$ tagged with one D_2, and (*C*) the composite of the two spectra. The spectra are essentially independent of the number of tags, allowing for the summation of the ion yields of all tagged species.

Fig. S5

Fig. S6. Vibrational predissociation spectra of D_2 tagged ions taken with the Berlin FEL (red trace, ≤1,000 cm^{-1}) and the Yale table top system (black, ≥1,000 cm^{-1}): (*A*) $H_3O^+(H_2O)_{20}$, (*B*) $D_3O^+(D_2O)_{20}$, (*C*) $Cs^+(D_2O)_{20}$, and (*D*) $Cs^+(H_2O)_{20}$.

Fig. S6

Fig. S7. Rotatable $H_3O^+(H_2O)_{20}$ structure I (B3LYP minimum).

Fig. S7

Fig. S8. Rotatable $H_3O^+(H_2O)_{20}$ structure II (MP2 minimum).

Fig. S8

Fig. S9. Rotatable $Cs^+(H_2O)_{20}$ structure.

Fig. S9

AUTHOR QUERIES

AUTHOR PLEASE ANSWER ALL QUERIES

Q: 1_PNAS mandates unambiguous pronoun antecedents. Please provide an appropriate noun after "This": "This corresponds to...."